Journal of Cleaner Production 277 (2020) 123834

Contents lists available at ScienceDirect

Journal of Cleaner Production

journal homepage: www.elsevier.com/locate/jclepro

Characterization of sugarcane bagasse ash as a potential supplementary cementitious material: Comparison with coal combustion fly ash

Ping Zhang [a, b], Wenyu Liao [b, 1], Aditya Kumar [c], Qian Zhang [d], Hongyan Ma [b, *]

[a] School of Civil Engineering, Qingdao University of Technology, Qingdao, Shandong, 266033, China
[b] Department of Civil, Architectural and Environmental Engineering, Missouri University of Science and Technology, Rolla, MO, 65401, USA
[c] Department of Materials Science and Engineering, Missouri University of Science and Technology, Rolla, MO, 65401, USA
[d] Department of Civil and Environmental Engineering, FAMU-FSU College of Engineering, Florida State University, Tallahassee, FL, 32310, USA

ARTICLE INFO

Article history:
Received 22 May 2020
Received in revised form
5 July 2020
Accepted 15 August 2020
Available online 24 August 2020

Handling Editor: Yutao Wang

Keywords:
Sugarcane bagasse ash
Coal-combustion fly ash
Characterization
Composition
Supplementary cementitious material

ABSTRACT

This study aims to evaluate the potential of sugarcane bagasse ash (SCBA) as a supplementary cementitious material (SCM) in terms of composition. Using coal-combustion fly ash (CFA) as the benchmark, SCBA is characterized thoroughly using multiple tools to determine and compare particle size, particle morphology, chemical composition, glass content, element distribution and chemical status. It is found that SCBA has fine particle size (d_{50} = 6.76 μm, compared to 2.2 μm of CFA), high glass content (78.5 wt%, compared to 81 wt% of CFA), and relatively stable chemical composition, making it a potential effective SCM. The glass content of SCBA is dominated by amorphous silica (77.2%, compared to 53.6% of CFA), which can lead to formation of secondary calcium silicate hydrates in pozzolanic reactions. However, SCBA contains no spherical glass grains but many porous grains, which may compromise the workability of fresh-state cement-based materials. Another two detriments of SCBA are high carbon and potassium contents, which could potentially interfere the performance of cement-based materials. However, due to their existence forms (i.e., either light or dissolvable, as revealed by X-ray photoelectron spectroscopy), these detrimental effects can be mitigated through washing. A literature-survey based analysis shows that the ash samples adopted in this study are representative, so the conclusions drawn from this study are generally meaningful.

1. Introduction

As one of the world's largest industrial solid wastes, coal-combustion fly ash (CFA), especially class C and class F according to ASTM C618 (ASTM C618-19, 2019), has been widely used in cement and concrete materials as a supplementary cementitious material (SCM) due to its technological advantages (Hemalatha et al., 2016; Rivera et al., 2015; Liao et al., 2017). These advantages include, but are not limited to (Shen and Zhang, 1981; Butler and Mearing, 1985; Ma, 2013): (1) spherical particle shape that can improve the fluidity of fresh-state cement-based materials; (2) filler effect, which provides additional nuclei for the formation of calcium silicate hydrates (C–S–H) and promotes cement hydration; and (3) pozzolanic effect, which leads to formation of secondary hydration products because of the reaction between CFA and cement hydrates, and, thus, results in improved mechanical and durability performance. CFA has actually become a key component for producing high-performance concrete. However, many countries have been facing shortages of CFA because of two-fold reasons. On the one hand, demand for concrete is ever-increasing because of the expansion and renovation of concrete infrastructure (Dhondy et al., 2019; Monteiro et al., 2017; Liao et al., 2019a), which has been enlarging the demand of CFA. On the other hand, many coal-fired power plants are retiring and environmental protection agencies have been continually issuing rigorous regulations to restrict the emissions of SO_2 and NO_x from coal-fired power plants (Fleischman et al., 2013; Duquiatan et al., 2020). As a result, supply of CFA is declining, and the fraction that cannot meet the technical requirements of ASTM C618 (ASTM C618-19, 2019) (i.e., off-specification CFA) is increasing. A recent initiative

* Corresponding author.
E-mail address: mahon@mst.edu (H. Ma).
[1] Contributed equally to the first author.

https://doi.org/10.1016/j.jclepro.2020.123834
0959-6526/

of the US National Cooperative Highway Research Program has even started to test the possibility of expanding the use off-specification ashes as SCMs for making concrete (TRB, 2018). To address such shortages of CFA and SCMs, as pointed out by a recent United Nations' report (Scrivener et al., 2018), geographically abundant minerals (e.g., calcined clay (LC3, 2014)) as well as locally and seasonally available minerals (e.g., natural pozzolans and rice husk ash (Juenger et al., 2011)) have to be fully leveraged.

Sugarcane bagasse ash (SCBA) is a typical locally available industrial byproduct. In a sugar-producing region, a large portion of the bagasse can be incinerated to generate power to run equipment for milling, clarification, evaporation and crystallization (Webber et al., 2016). SCBA is the residue of this incineration process. Although the percentage of ash only represents less than 3% of the original mass of the bagasse, the large volume of combusted bagasse can generate massive amount of SCBA that has to be handled economically and eco-friendly (Webber et al., 2016). In Louisiana – an important sugar-producing area in the US – the annual production of SCBA is up to 40,823 metric tons; and based on the numbers projected in (United Staes Department of Agriculture, 2015), around 5 million metric tons of SCBA can be produced globally every year. This does not represent an amount that is large enough to replace CFA. However, if SCBA can be scientifically utilized, it can serve as a renewable resource to partially compensate the local shortage of SCMs (Rovani et al., 2018; Usman et al., 2014). Some attempts have been made to test the possibilities of using SCBA as an SCM (Dhengare et al., 2015; Moraes et al., 2015; Rerkpiboon et al., 2015; Bahurudeen et al., 2015; Ganesan et al., 2007) and a precursor for alkali-activated materials (Castaldelli et al., 2013; Pereira et al., 2015). In SCM-oriented studies, some researchers have reported positive effects of SCBA on pore structure, strength, impermeability and durability (Dhengare et al., 2015; Rerkpiboon et al., 2015; Ganesan et al., 2007), while some have identified negative influences of SCBA on fresh-state, early-age, and even long-term properties (Moraes et al., 2015; Bahurudeen et al., 2015). Inconsistency in the literature can be attributed to the chemical or compositional variance of SCBA, since the studies just used a local ash with random chemical composition.

Recognizing the chemical composition, mineral composition, surface functional groups, reactivity and physical properties of an ash is of great significance for maximizing its beneficial use in cement-based materials – as an SCM (Ma, 2013; Liao et al., 2019b). In recent years, a certain amount of studies have been published on the characterizations of either CFA (Chancey et al., 2010; Deng et al., 2016; Ha et al., 2016; Ohki et al., 2005; Ibáñez et al., 2013; Yan et al., 2018; Singh and Subramaniam, 2016) or vegetable ashes (Imran and Khan, 2018; Agredo et al., 2014). Various test methods have been utilized individually or in combination for the sake of characterization. Typically, x-ray fluorescence (XRF) is used to characterize oxide compositions of ashes. Quantitative x-ray diffraction (QXRD: Rietveld analysis of XRD patterns) is employed for determining the crystalline phase contents, while the glass contents of ashes can be obtained by subtracting the oxide equivalent of crystalline phase contents from the overall oxide compositions (Le Saoût et al., 2011). Furthermore, the unburnt carbon content is normally measured by testing the loss on ignition (LOI, mass loss in a sample heated to 950 °C according to ASTM D7348 (ASTM D7348-13, 2013)) of the ashes. Lastly, if the particle size distribution and specific surface area of the ashes are of interest, they can be quantified using laser particle size analyzer (Wyatt, 1980) and nitrogen adsorption (Külaots et al., 2004), respectively. However, these methods, although well-established and widely used, have their limitations. For example, the LOI measurement does not distinguish unburned carbon from other thermally decomposable ingredients (e.g., crystalline carbonates and hydroxides); for a vegetable ash, like SCBA, it tends to overestimate the content of unburned carbon. Furthermore, these methods do not tell chemical states of elements (e.g., carbon) and may not be able to characterize other light elements. To solve these issues so as to characterize the composition of SCBA, other techniques such as X-ray photoelectron spectroscopy (XPS) would need to be used to complement the aforementioned characterization protocol (Rajamma et al., 2009).

Developed based on the concept that photoelectrons released from the surface of a sample – irradiated with soft X-rays – have different kinetic energies, XPS is a surface-sensitive quantification technique to determine chemical composition as well as chemical states of elements (Deng et al., 2016; Fu et al., 2018). Since XPS probes only less than 20 nm into the sample (Rajamma et al., 2009; Fu et al., 2018), it tends to overestimate the contents of adventitious elements, such as carbon due to carbonation effect and contamination during production. To avoid surface carbonation effect on samples for XPS test, researchers have proposed to either use fresh surfaces in the test (Vander Wal et al., 2011), or create a carbon-free environment for sample preparation (Deng et al., 2016). However, regarding to an industry waste like SCBA, as-received powder already has small particle sizes and has been exposed to air for a long time. It is therefore inefficient to further grind SCBA into smaller sizes so as to get fresh surfaces, and it is meaningless to maintain the sample in carbon-free environment. SCBA does contain unburned carbon, but it is unclear if the carbon is embedded in ash grains or exists as small particles (as either separate particles or adhering on the surface of ash grains) (Joyce et al., 2006; Liu et al., 2011). Therefore, special concerns (for both sample preparation and data analysis) should be taken for XPS characterization of SCBA, and quantitative deconvolution based on high-resolution XPS spectra (e.g., C1s, O1s and K2p) could be used for the purposes of improving the accuracy of analysis as well as identifying surface functional groups and chemical states (Fu et al., 2018). Some XPS studies of biomass ashes in the literatures (Agredo et al., 2014; Pande et al., 2012; Subramanian et al., 2013) have focused on fitting carbon spectra; however, on an XPS spectrum, the peaks of carbon and potassium (i.e., C1s and K2p) overlap with each other (Fairley, 2009). Given that the unburned carbon content of a biomass or vegetable ash is typically higher than 2% and the potassium content ranges generally from 3.2% to 8.7% (Agredo et al., 2014; Rajamma et al., 2009; Souza et al., 2011), the overlap has to be solved for accurate composition characterization.

The present study aims to comprehensively characterize SCBA. Instead of qualitative or semi-quantitative characterizations in many past studies (Imran and Khan, 2018; Agredo et al., 2014), this study leveraged multiple technologies to achieve quantitative characterizations of chemical compositions of surface and interior of SCBA grains. In addition to standard methodologies, this work combines XRF and QXRD to elucidate the overall chemical composition and the composition of the glass phase; scanning electron microscopy (SEM) coupled with energy dispersive x-ray spectroscopy (EDS) and XPS are combined to examine the status and distribution of some elements (e.g., carbon); and synchronous deconvolution of overlapping carbon and potassium peaks is employed for the first time for more accurate characterization of SCBA. The characterization of SCBA is carried out in comparison with a CFA. Based on the results as well as literature analysis, the feasibility of using SCBA as an SCM in concrete is discussed.

2. Experimental methods

The main experimental work in this paper is to investigate the elemental and phase composition as well as chemical bonds of two types of silicoaluminate ashes. One is an SCBA produced from

burning of sugar cane bagasse in Louisiana, and the other is an ordinary class-F CFA, generated from coal combustion at a local (Missouri) electric power plant. As received, the SCBA in the form of powder has a grey color closed to that of the conventional CFA. The skeleton density of the SCBA is 2.53 g/cm^3, which is similar with that of 2.35 g/cm^3 of the CFA. However, the bulk density of the SCBA is 0.49 g/cm^3, much smaller when compared with that of 0.98 g/cm^3 of the CFA. As introduced in section 1, standard methods were followed to characterize the particle size distribution and LOI of the ashes, XRF and QXRD were combined for compositional analyses, and XPS measurement was carried out to reveal more details of some elements. The compositions obtained by XPS were also compared with the results of XRF, to reveal the phase distribution in ash grains assisted by SEM/EDS.

2.1. Particle size distribution

Particle size distributions of the two ashes were analyzed using a Microtrac S3500 Particle Size Analyzer (Microtrac Inc., Montgomeryville, USA), using the principle of laser diffraction. The instrument was equipped with three precisely placed red laser diodes to accurately measure sizes of particles in the range of 0.02−2800 μm. Before collecting data, a 60-s ultrasonication was implemented by the built-in sonicator to help with dispersion of the powder samples in the liquid media of isopropanol. Particle size distributions of the two types of ashes were determined before and after 15-s grinding using a disc mill. The grinding was for detailed XPS analysis as will be introduced in section 2.5. To further breaking the ash grains and maintain the freshness of the exposed surfaces, grinding was carried out in a nitrogen-filled glove box and immediately stored in sealed sample bags until particle size analysis and XPS testing were performed.

2.2. Loss on ignition (LOI)

The CFA and SCBA samples were firstly oven-dried and then burned to a constant weight at 950 °C to determine their loss on ignition (LOI). The test procedure conformed to ASTM D7348.

2.3. X-ray fluorescence spectrometry (XRF)

The oven-dried samples were scanned using an X-Supreme 8000 Energy Dispersive X-ray Fluorescence Spectrometer (Oxford Instruments, Abingdon, UK). The scans were conducted in 40 mm aluminum cups that were standard for the powder sample analysis. The measurement time was 200 s.

2.4. Quantitative x-ray powder diffraction (QXRD)

X-ray diffraction (XRD) data of the oven-dried powder samples were collected by a PANanalytical X'pert Pro MPD diffractometer, using CuKα radiation ($\lambda = 1.54$ Å) and an X-Celerator solid detector. The patterns were examined at room temperature with 2θ ranging from 10° to 70°. The step size was $\Delta 2\theta = 0.02626°$, and the time per step was 200s. That means a scan speed of 0.03348°/s owing to the use of strip detector with 255 active channels. As a result, a total counting time for each sample was about 45 min. The phase compositions were identified with the assistance of X'Pert HighScore Plus software. Al_2O_3 (α) was added to the samples as internal standard to quantify the crystalline and amorphous phases in the samples, since there was no Al_2O_3 (α) peak was found in the original spectra. Based on the XRD patterns, the Rietveld method was used to quantitatively analyze the crystal and amorphous phases in the samples.

2.5. X-ray photoelectron spectroscopy (XPS)

XPS analysis for the ash samples was performed with a Kratos Axis Ultra DLD Spectrometer (Kratos Analytical Ltd., Manchester, UK) equipped with a MgKα X-ray source (1253.6 eV, 150 W). The analysis chamber was maintained at high vacuum − $5 \times I0^{-8}$ Torr or lower − during the analysis. Survey scan analyses were carried out within a spot size of 700×300 μm^2 area and a pass energy of 30eV. High-resolution scan analyses were performed to obtain the spectra of C1s, K2p and O1s. The energy step size for the narrow scan analysis was 0.05 eV. The final high-resolution scan spectrum was obtained with three cycles of scanning for each element. Least-square curve-fitting analyses of C1s, K2p and O1s spectra were carried out with a Gaussian/Lorentzian (70/30) product function using the CasaXPS program. Mole fractions were calculated using peak areas normalized on the basis of acquisition parameters after linear Shirley background subtraction. To compensate the shifts in binding energy (BE) due to charging, the observed binding energies were all corrected by setting the BE value for the C1s peak of carbon in the sample to be 284.5 eV. In addition, to reveal the distribution of elements in the ash grains (e.g., surface-rich or uniformly distributed), a group of ground samples were also scanned and compared with the unground samples.

2.6. Scanning electron microscopy (SEM)

The morphologies of the grains of the two ashes were investigated with a field emission scanning electron microscope (S4700 FE-SEM, Hitachi, Japan). The ashes were oven dried to constant weight before sample preparation. The sample particles were sprayed on a carbon tape and subjected to gold coating for the SEM observation. They were imaged with 15 kV accelerating voltage and 10 μA emission current in secondary electrons detecting mode. The powder samples were also mounted in resin, which were then polished following a well-established procedure (Hu and Ma, 2016) to expose cross-sections of the ash grains. The polished surfaces were coated with Au−Pd and observed under backscattered electron (BSE) detecting mode with 30 kV accelerating voltage and 15 μA emission current. The BSE imaging was assisted by energy dispersive x-ray spectroscopy (EDS) to analyze the distribution of elements in the ash grains.

3. Results and discussion

3.1. Particle size distribution

The particle size distributions of the two types of ashes before and after grinding are shown in Fig. 1. The characteristic particle diameters and specific surface areas of the raw and ground ashes are given in Table 1. In Fig. 1 and Table 1, it can be seen that the particle size distributions of the two raw ashes are fairly different. The SCBA appears to be coarser than the CFA. The particles sizes of both ashes decline obviously after grinding, and the change of SCBA is more significant. According to Table 1, the mean particle size (d_{50}) of the CFA falls from 2.22 μm to 1.65 μm after grinding (26% reduction); as for the SCBA, this value descends from 6.76 μm to 3.36 μm (50% reduction). Meanwhile, the specific surface areas of the ground CFA and the ground SCBA are around 36% and 98% larger than the raw ashes, respectively. Given that the grinding energy for both ashes were comparable, the extends of particle size variation due to grinding implies that the SCBA grains are more fragile than the CFA grains. This further implies two aspects, as compared with CFA: (1) SCBA may be detrimental to the mechanical properties of cement-based materials; and (2) if grinding is employed to yield finer binder for reactivity improvement (Bahurudeen et al., 2015;

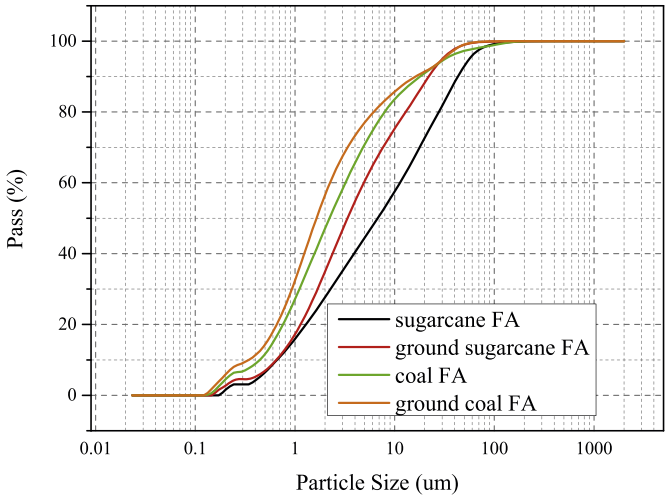

Fig. 1. Particle size distributions of the raw and ground SCBA and CFA.

Table 1
Characteristic particle diameters and specific surface areas of the raw and ground ashes.

	d_{10} (μm)	d_{50} (μm)	d_{90} (μm)	Specific surface area (m^2/cm^3)
CFA	0.445	2.223	18.07	0.773
Ground CFA	0.344	1.646	16.26	1.052
SCBA	0.661	6.76	43.10	0.378
Ground SCBA	0.650	3.36	22.05	0.747

Cordeiro and Kurtis, 2017; Cordeiro et al., 2009, 2019), SCBA requires less grinding energy.

3.2. Compositional analyses

The LOIs of SCBA and CFA samples were firstly determined. Regarding to combustion ashes in which unburned carbon is presented, LOI has long served as a parameter to represent unburned carbon content (Chancey et al., 2010). LOI is also used to correct XRF results or as a pretreatment of XRF test for compositional analyses. Though LOI may overestimate the unburned carbon content, as discussed in section 1, the traditional combining strategy of LOI and XRF is still adopted in this section. The LOI and XRF test results of the SCBA and CFA are shown in Table 2.

From Table 2, it can be seen that the oxide/element types in the CFA and SCBA are quite consistent. The (SiO_2+Al_2O_3+Fe_2O_3) contents of them are 84.4% and 87.3%, respectively. However, the composition of CFA is dominated by SiO_2 (56.31%) and Al_2O_3 (23.21%), while that of the SCBA is dominated by SiO_2 (76.16%). The CaO content of the CFA is 9.73%, meaning that the CFA may have limited hydraulic reactivity, apart from pozzolanic reactivity, when being used as an SCM in Portland cement based materials. Its total alkali content, measured by equivalent Na_2O content (Na_2O_{eq} = % Na_2O + 0.658 × %K_2O) (ASTM C1778-19b, 2019), is at a relatively low level (i.e., 0.74%). Summarizing the chemical composition, LOI (i.e., 0.87%) and fineness, the CFA tested in this study appears to be a high-quality class F fly ash (ASTM C618-19, 2019). The high SiO_2 content of the SCBA, if proven to be mainly amorphous by XRD, guarantees that this material can potentially show pozzolanic reactivity. However, its low CaO content (i.e., 2.32%) indicate that the hydraulic reactivity of the SCBA could be negligible. As compared to the CFA, the SCBA has a high K_2O content (i.e., 3.97%), which makes its equivalent Na_2O content be as high as 2.8%. That is to say, as a potential SCM, the SCBA needs to be used at relatively low replacement levels or with special treatment; otherwise, it may expose the concrete to a relatively high risk of alkali-aggregate reaction (ASTM C1778-19b, 2019). Another essential difference between the two ashes is that the SCBA has a LOI of 2.46%, which is almost tripled that of the CFA. The LOI may be governed by unburned carbon, which could interfere negatively with the performance of concrete (especially fresh-state properties) and will be further investigated in sections 3.4 and 3.5. Other minor oxides (e.g., MgO, P_2O_5, SO_3 and TiO_2) and trace level elements (e.g., Sr, Zn, Cr, and Cl) are not expected to significantly affect the performance of the ashes as SCMs in cement-based materials.

Table 2
Chemical compositions of CFA and SCBA, wt% (mg/kg if marked by *).

Composition	CFA	SCBA
Na_2O	0.05	0.19
MgO	1.68	1.47
Al_2O_3	23.21	8.38
SiO_2	56.31	76.16
P_2O_5	0.15	1.49
SO_3	0.71	0.24
K_2O	1.05	3.97
CaO	9.73	2.32
Mn_2O_3	0.11	0.13
Fe_2O_3	4.88	2.71
TiO_2	1.09	0.42
SrO	0.12	233*
ZnO	112*	175*
Cr_2O_3	189*	90*
Cl	206*	80*
LOI	0.87	2.46

3.3. X-ray diffraction (XRD) analysis

To identify and quantify phases in the SCBA and CFA, quantitative XRD tests were implemented and the representative diffraction peaks for each phase are labeled in Fig. 2. It can be seen that peaks representing quartz (SiO_2, ICSD 27831) and mullite ($Al_{4.54}Si_{1.46}O_{9.73}$, ICSD 66450) are easily identified in the CFA diffraction pattern, which is consistent with most of class F ashes (Chancey et al., 2010; Ibáñez et al., 2013; Yan et al., 2018; Singh and Subramaniam, 2016). The main crystalline phases presenting in the SCBA diffraction pattern are quartz (ICSD 27831) and anorthite ($CaAl_2Si_2O_8$, ICSD 23922), and a very low amount of cristobalite (SiO_2, ICSD 35536) can also be detected. This indicates that Ca could more readily enter the Si—O/Al—O tetrahedral lattice to form anorthite instead of

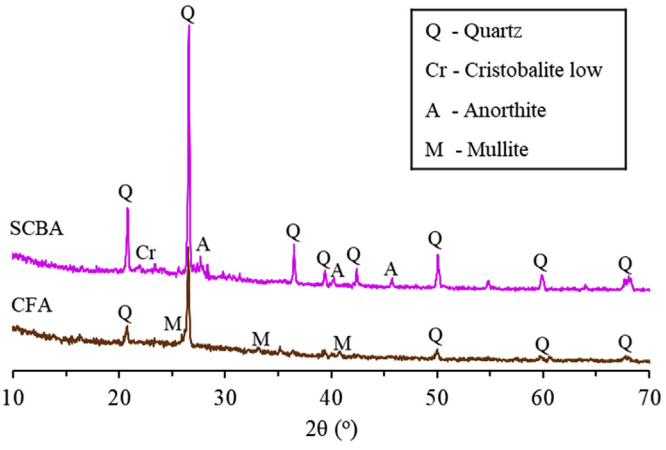

Fig. 2. XRD diffractograms of CFA and SCBA.

mullite during the formation of SCBA compared with CFA, but the specific mechanism behind it needs to be further explored. Moreover, apart from the major phases labeled in Fig. 2, possible trace phases are also given in Table 3. These phases may exist according to existing literatures and the obtained XRD patterns, whereas their existence cannot be determined for sure because of peaks overlapping or their limited amounts. In Fig. 2, humps within the 2θ range of 20°–40° are noticeable in both samples, which indicate their high amorphous contents (Chancey et al., 2010). Given that Rietveld analysis is a mature technique widely used to perform a full-component quantitative phase analysis from the XRD pattern, relative proportions of crystalline phases as well as amorphous phases in the CFA and SCBA are acquired via Rietveld refinement method and the obtained results are shown in Table 3.

According to Table 3, both the SCBA and the CFA have large percentages of amorphous phases, and the two percentages are 78.5% and 81% for SCBA ad CFA, respectively. Subtracting the crystalline phases in Table 3 (i.e., SiO_2 and $Al_{4.54}Si_{1.46}O_{9.73}$) from the chemical compositions shown in Table 2, the composition of the amorphous phases of SCBA and CFA can be estimated. The calculations yield that the amorphous phase in the SCBA is dominated by SiO_2 (60.6% of the ash, or 77.2% of the amorphous phase) and Al_2O_3 (6% of the ash, or 7.6% of the amorphous phase), and that in the CFA is also dominated by SiO_2 (43.4% of the ash, or 53.6% of the amorphous phase) and Al_2O_3 (17.8% of the ash, or 22% of the amorphous phase). In other word, if the two ashes are used as SCMs in cement-based materials, the pozzolanic reaction of the CFA will form considerable amounts of aluminate hydrate in addition to secondary C–S–H (Thomas et al., 2017; Massazza, 1998; Shi and Day, 2000), while the reaction products of SCBA will be mainly secondary C–S–H.

3.4. XPS analysis

XRF is commonly used in semi-quantitative or quantitative elemental analysis for inorganic minerals. Although the most advanced XRF claims to be able to measure the amounts of carbon and other light elements as well as low-concentration elements, the sensitivity may not be satisfactory (Frey et al., 2011). In principle, XRF has good sensitivity and accuracy only when determining contents of relatively heavy elements with high-enough concentration (Reyes-Herrera et al., 2015). In this section, another elemental analysis technical – XPS – is adopted to quantify the major (e.g., Si and Al), minor (e.g., Mg and K), and trace elements (e.g., Ti, Sr, Zn, Cr, and Cl) in the SCBA and CFA. The effect of particle breaking on test results of XPS is investigated, and the results are compared with that of XRF. The capacity of XPS in identifying the surface element states or functional groups is also discussed.

3.4.1. Effect of particle grinding on XPS results

Based on XPS results, the bimodal binding energy difference combined with the peak positions are used for presence confirmations and quantitative determinations of the major, minor and trace elements in the SCBA and CFA (before and after grinding), as shown in Fig. 3. The quantitative results are listed in Table 4.

Table 4 compares the XPS results of the two ashes before and after grinding, and the differences (measured by weight percentage of the raw ash) induced by the grinding (or particle breaking) are also listed. If an element distributes uniformly throughout (i.e., from the interior to the surface of) the particles, the obtained difference should be zero or very small. This type of elements include O, Ca, Al and K in both ashes. A negative difference indicates that the element is rich in the surface layer of the particles, especially the first 20 nm as introduced in the introduction section. Such elements, such as Na, S and C in the CFA and Fe and P in the SCBA, can be diluted due to the breaking of particles. On the contrary, a positive difference may indicate the element is lean in the surface layer but relatively rich beneath the first 20 nm. Examples of this category are Mn in both ashes and Mg in the CFA. Many of these

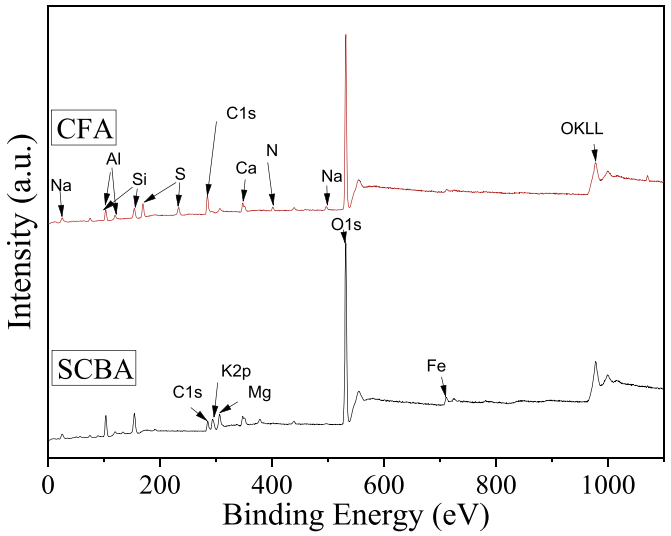

Fig. 3. XPS broad spectra of elements in raw SCBA and CFA.

Table 4
XPS surface chemical composition of the raw and ground ashes (wt%).

	CFA	Ground CFA	Diff.(%)	SCBA	Ground SCBA	Diff.(%)
C 1s	12.01	10.34	−13.91	5.26	8.03	52.7
N 1s	1.52	1.21	−20.39	–	0.07	–
O 1s	49.53	49.85	0.65	50.46	49.84	−1.23
Na 1s	1.14	0.69	−39.47	0.31	0.31	0
Mg 2s	0.31	0.59	90.32	1.38	1.28	−7.25
Al 2p	6.22	6.85	10.13	3.69	3.23	−12.47
Si 2p	12.39	14.84	19.77	22.69	23.52	3.66
P 2p	0.11	0.39	255	1.54	0.94	−38.96
S 2p	9.44	7.83	−17.06	0.24	0.28	17
Cl 2p	0.21	0.3	42.86	0.1	0.11	10
K 2p	0.26	0.27	3.85	4.53	4.03	−11.04
Ca 2p	3.86	4	3.63	4.39	3.95	−10.02
Ti 2p	0.25	0.43	72	0.2	0.09	−55
Cr 2p	0.6	0.29	−51.67	0.41	0.38	−7.32
Mn2p	0.16	0.29	81.25	0.28	0.57	104
Fe 2p	1.58	1.74	10.13	3.88	2.87	−26.03
Zn 2p	0.35	0.07	−80	0.51	0.25	−50.98
Sr 3p	0.08	–	–	0.09	0.24	167

Table 3
Relative proportions of crystalline and amorphous phases in CFA and SCBA achieved by Rietveld method (wt%).

	Quartz	Mullite	Anorthite	Amorphous	Other possible phases[a]
CFA	11.3	7.7	–	81	α-Fe_2O_3 (Ha et al., 2016), ettringite, maghemite, periclase, anatase (Chancey et al., 2010)
SCBA	14.4	–	7.1	78.5	Calcite (Dhengare et al., 2015; Souza et al., 2011), ferric oxide (Dhengare et al., 2015), microcline (Souza et al., 2011)

[a] It is estimated that the total amount of these trace phases does not exceed 5%.

elements follow opposite trends of changing due to grinding (i.e., being exposed to a larger extent), because of their different distributions probably attributed to their process of formation. Carbon serves as a good example to demonstrate this. In the formation process of CFA, unburned carbon exists as nano/submicron particles in the flue gas, which then precipitate on the surface of aluminosilicate glass grains during cooling (Drozhzhin et al., 2018; Żyrkowski et al., 2016; Zevenbergen et al., 1999; Kutchko and Kim, 2006); therefore, carbon is a surface-rich element in CFA (denoted by a "-" difference in Table 4). During combustion of sugarcane bagasse, although nano/submicron particles of unburned carbon can also be formed and precipitate on aluminosilicate particles, some micro-scale gains of insufficiently burned carbon particles could form too in the forms of plain carbon or carbon-aluminosilicate solid solutions. This hypothesis will be tested in section 3.5 in the light of BSE/EDS. If validated, this theory also explains why the SCBA appears to be more fragile than the CFA, as explored in section 3.1.

3.4.2. Comparison between XPS surface analysis and XRF bulk analysis

In this section, the elemental compositions of the SCBA and CFA determined by XPF and carbon content determined by LOI are plotted in Fig. 4 along with the XPS results. The carbon contents determined by XPS of the two ashes are both significantly higher than that determined by XRF/LOI, further confirming the surface enrichment of carbon in the ashes (all CFA particles and part of SCBA particles, according to section 3.4.1). With such significant overestimation of carbon, the other elements should tend to be underestimated by XPS, as demonstrated by most of the elements in CFA [see Fig. 4(a)]. The exceptions, such as S, N and Na, are other surface-rich elements in CFA, which is consistent with Table 4 (illustrated by the "-" differences of these elements). As shown in Fig. 4(b), there are more exceptions in the SCBA, including Fe, Ca, K, P, and Mg. This is not out of expectation because all of them have "-" differences in Table 4, indicating that these elements probably have characteristics of enrichment at the surface layer of the SCBA grains. It should be noted that these conclusions are based on the assumption that the ash samples have been mixed well and particles in each sample have similar distributions of chemical compositions. To further substantiate these claims, more detailed discussion based on SEM/BSE and EDS observations will be presented in Section 3.5.

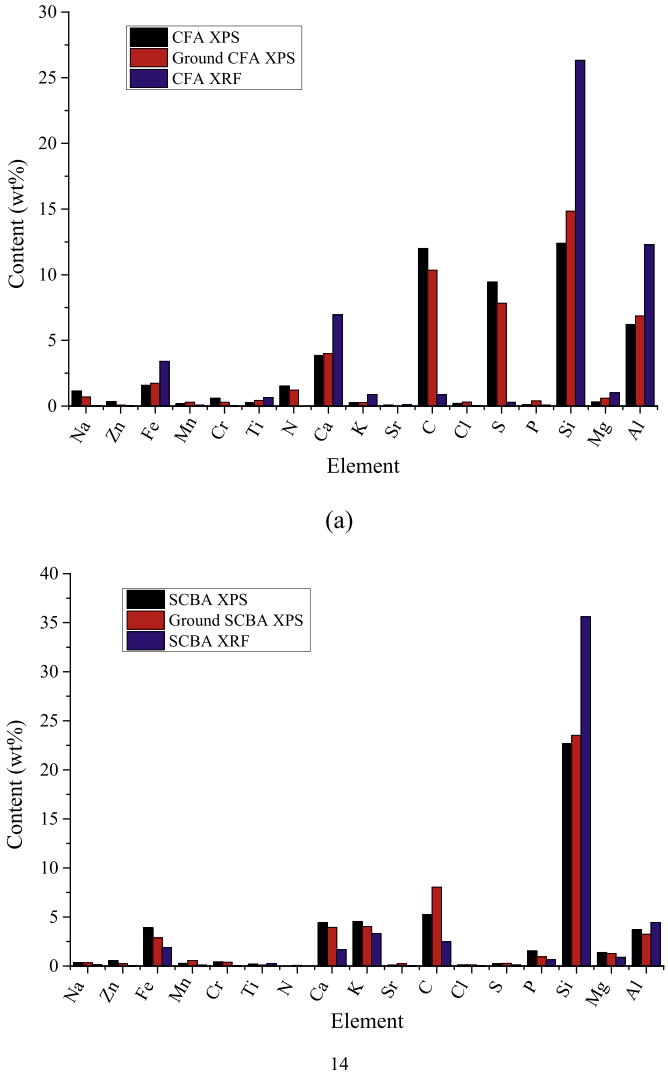

Fig. 4. Comparisons between the element proportions extracted from XRF and XPS tests: (a) CFA samples; (b) SCBA samples.

3.4.3. Chemical states of carbon, potassium and oxygen on surface of ash grains

Chemical states analysis and surface functional groups identification are complementary to elemental characterization based on XPS. Since carbon is the most predominant surface-rich element, high-resolution scans are implemented to identify its states and C-involving surface functional groups. Because of the potential overlapping of K2p and C1s and the association of oxygen with carbon in forming functional groups, the states of surface potassium and oxygen are also analyzed based on deconvolution. The fitting results are displayed in Fig. 5 and Fig. 6.

Fig. 5 shows high-resolution scans over the nominal C1s and K2p regions (i.e., 281–299 eV) for the two ashes and the corresponding deconvolution fittings. The characteristic peaks of selected function groups and bonds generate well-fitting curves, which enables the interpretation of the overlap between the C1s and K2p peaks. It can be seen that the K2p peak exhibits great asymmetry probably due to its formation of various functional groups and bonds with carbon and other elements/groups. The curves are fitted as previously described in Section 2.5 to extract information on the carbon and potassium bonding as well as

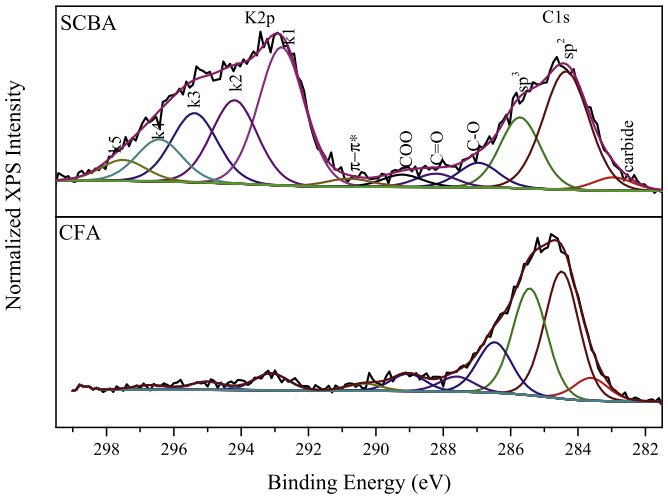

Fig. 5. High-resolution scan results for C1s and K2p for the SCBA and CFA.

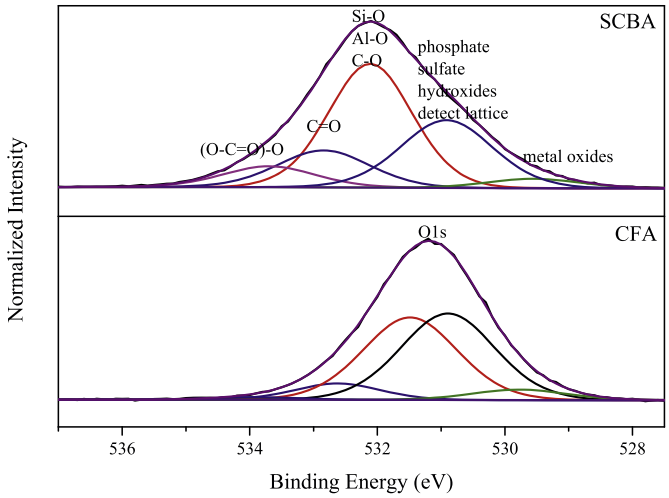

Fig. 6. High-resolution O1s XPS spectra of the SCBA and CFA.

functional groups. The assignments of C1s and K2p peaks have been well-referenced in the database and literatures (Vander Wal et al., 2011; Subramanian et al., 2013; Naumkin et al., 2012). As illustrated in Fig. 5, seven carbon peaks observed at the binding energy regions of 283, 284.5, 285.4, 286.4, 287.4, 288.6 and 290 eV are corresponding to carbide, sp2, sp3, C–O, C=O (carbonyl), COO (carboxyl) and π–π* transitions, respectively. Five potassium peaks pinned at the locations of 293.0, 293.8, 294.9, 296.5 and 297.8 eV can be assigned to different matters as shown in Table 5. A conclusion can be drawn that the potassium in SCBA has two major chemical states. One is to bind with carbon and occupy a tetrahedral or octahedral position of graphite intercalation compounds (GIC), and the other is to combine with oxygen and form phosphates, sulfates, as well as oxides. The former state has a general form of K_xC, which is typically formed by the intercalation of potassium atoms into the graphite layer (Murakami et al., 1990). If intercalating particles – potassium atoms in this case – form covalent bonds with graphite, the conjugated sp^2 system of graphite is destroyed, usually forming sp^3 Estrade-Szwarckopf, 2004. These analyses can be mutually confirmed by the peak fitting results of the C1s spectra as shown in Fig. 5. As compared with SCBA, the CFA contains much less potassium, which is consistent with Table 4 and Fig. 4, and the majority of potasssium is in the forms of dissolvable salts (e.g., phosphate and sulfate) and/or oxide. Furthermore, the major forms of carbon in the CFA could also be graphite (or GIC), as proven by the dominant sp^2 and sp^3 peaks in Fig. 5, but the overall carbon content is lower. The discrepancy of content and states of carbon and potassium between SCBA and CFA could be intimately related to their different formation processes (e.g., sugarcane, as a vegetable product, contains much more potassium and hydrocarbon than coal), which is out of scope of the present study. The analysis of chemical states of carbon and potassium provides a reference for potential removal of these matters for quality control of SCBA, as an SCM (e.g., to prevent alkali-aggregate reaction induced by excess potassium).

Fig. 6 presents the O1s XPS spectra of the two samples. The O1s binding energy peak can be decomposed into five different oxygen environments. The peak at around 532.0 eV is assigned to Si/Al–O (Deng et al., 2016; Joyce et al., 2006; Naumkin et al., 2012), whose proportion is the highest (approximately 50%). This is reasonable since SiO_2/Al_2O_3 are the major components of the glass phase of both ashes. The peak at around 531.0 eV contains SO_x and PO_x (Agredo et al., 2014; Naumkin et al., 2012), part of which are associated with potassium as discussed above. In addition, the peaks at about 530eV, 532.8eV and 533.8 eV correspond to metal oxides (Fu et al., 2018), C=O (Naumkin et al., 2012; Pereira et al., 2014)and (O–C=O)–O (Deng et al., 2016; Naumkin et al., 2012; Pereira et al., 2014), respectively. The major difference between the two ashes that can be seen from the O1s spectra is that the SCBA contains much more C=O and (O–C=O)–O groups, because of the organic origin of SCBA.

3.5. SEM, BSE and EDS investigation

3.5.1. Grain morphology

The morphologies of the SCBA and CFA grains are depicted in Fig. 7. It can be seen that the particle sizes of both ashes are from submicron to more than 20 μm, consistent with Fig. 1. The majority of the CFA are well-rounded spherical particles (Xu and Shi, 2018), while most SCBA particles are in irregular shapes (i.e., prismatic, fibrous, etc.) with different sizes. This difference can be attributed to the relatively low combustion temperature reached in the burning process of SCBA, which may not be high enough to melt as much melted inorganic matters as in CFA (Kutchko and Kim, 2006). As suggested by the grain morphology, when being used as an SCM, the SCBA may not be able to improve the rheological performance of fresh state cement-based materials as CFA, because of the lack of ball-bearing effect (Neville, 2011).

3.5.2. Intra-grain structure and element distribution

Fig. 8 shows the polished cross-sections of several SCBA grains and the corresponding element distributions obtained from EDS analysis. It can be seen that the SCBA consists of solid grains and porous grains. The solid grains are dominated by silicon and oxygen, so they should be the amorphous SiO_2 phase as shown in sections 3.2 and 3.3. In Fig. 7(c) and (d), one can easily find some porous and fragile particles, to which the big porous grain in Fig. 8 belongs. These particles should be where carbon is rich. The brightest areas in the C-mapping are attributed to epoxy, apart from which carbon is also rich in the porous grain. The porous grain also contains aluminium, silicon, potassium and oxygen, and, thus, it appears to represent a solid solution of silicoaluminate glass, unburned carbon (likely graphite as shown in section 3.4), and minor element (e.g., potassium). The mappings are consistent with the XPS results in section 3.4 – the porous grains rich in carbon is more likely to break during the grinding process, resulting in a relatively large amount of carbon being exposed on the surface of

Table 5
Binding energy and parameters used for fitting K2p signals (Naumkin et al., 2012).

	Binding energy (eV)	Assignment/Formula	Remarks
K1	293.0	actinolite/$(K,Ca)_2$ $[Mg_{4.3}Fe_{0.7}][Si_{7.2}Al_{0.8}O_{22}](OH)_2$ K_2SO_4, K_3PO_4	Ca, Mg, Fe, K combined with $[Si/AlO_4]$ tetrahedron, Phosphate and Sulfate
K2	293.8	$K_xC/K_{1.4}C_{60}$, $K_{2.0}C_{60}$, $K_{2.7}C_{60}$, $K_{2.8}C_{60}$	K^+ ions occupying octahedral sites (K2p3/2)
K3	294.9	$K_xC/K_{1.4}C_{60}$, $K_{2.0}C_{60}$, $K_{2.7}C_{60}$, $K_{2.8}C_{60}$	K^+ ions occupying tetrahedral sites (K2p3/2)
K4	296.5	$K_xC/K_{0.8}C_{60}$, $K_{1.4}C_{60}$, $K_{2.0}C_{60}$, $K_{2.7}C_{60}$	K^+ ions occupying octahedral sites (K2p1/2)
K5	297.8	$K_xC/K_{0.8}C_{60}$, $K_{1.4}C_{60}$, $K_{2.0}C_{60}$, $K_{2.7}C_{60}$	K^+ ions occupying tetrahedral sites (K2p1/2)

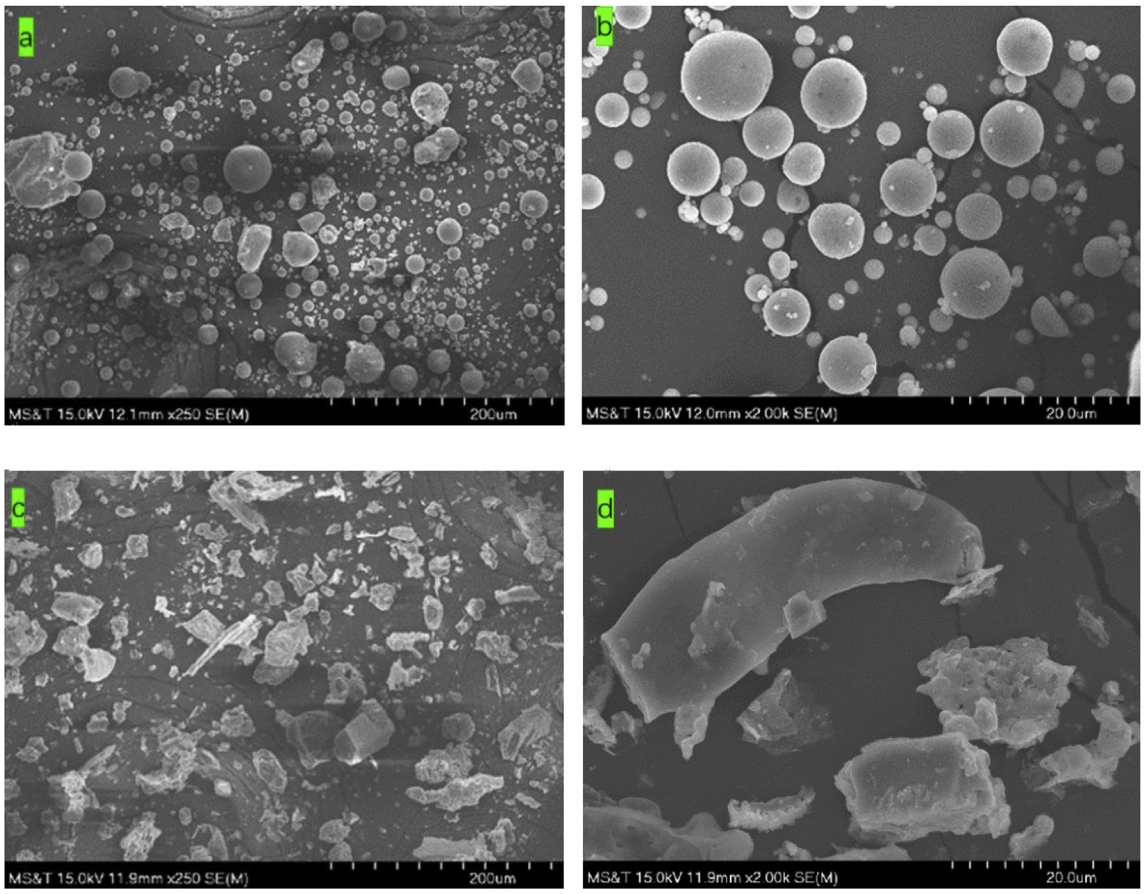

Fig. 7. Morphologies of the ash grains: (a, b) CFA and (c, d) SCBA.

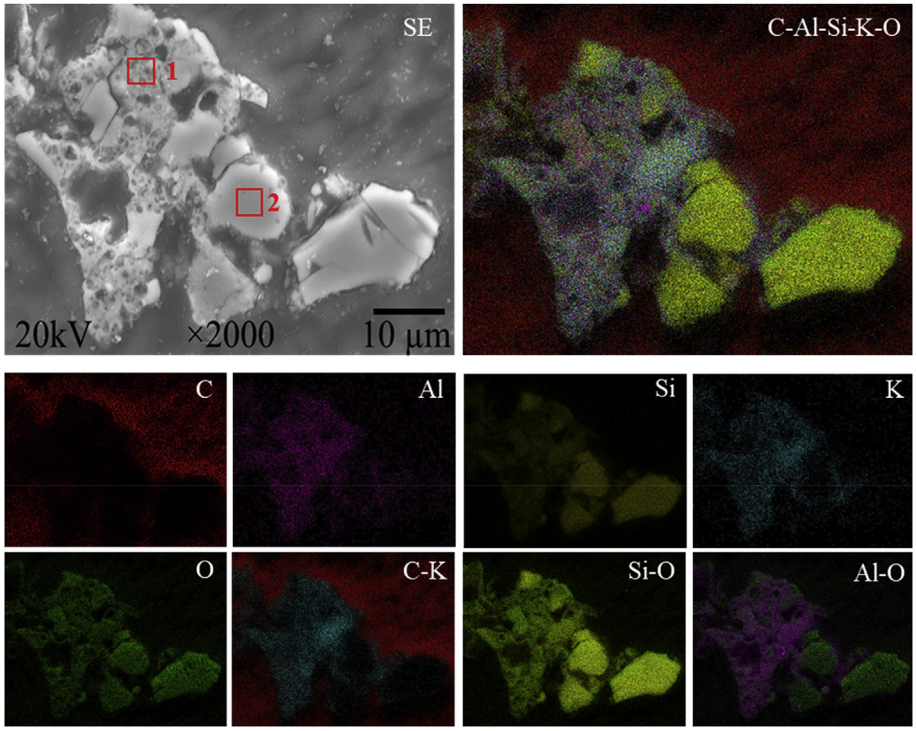

Fig. 8. SEM image of SCBA grains and corresponding element mappings based on EDS.

the particle after grinding (see Table 4 and Fig. 4).

Fig. 9 presents the polished cross section of an individual CFA particle and corresponding EDS mappings of four elements. It can be seen that Ca, Si and Al are uniformly distributed through the grain, and no obvious signals of carbon can be observed in the particle. If carbon is rich on the surface, it may be difficult to judge based on these mappings since the carbon signal out of the grain has been dominated by epoxy. Moreover, there is a drawback of relatively low resolution for the elementary mappings, which may miss small enrichment tendency. Thereby, an EDS line scanning is conducted to semi-quantitatively characterize the distribution of elements along the white line shown in Fig. 10. It shows a clear tendency of surface carbon enrichment, while Al, Si, and Ca show an internal enrichment tendency which is consistent with the mapping results in Fig. 9. This is also in accordance with the XPS and XRF analysis results discussed in Section 3.3.

3.6. Discussion on utilization prospects of SCBA

A SCBA and a typical class F CFA are characterized thoroughly and compared in this study. Assuming that the chemical variation of sugarcane bagasse is small, the variation of chemical composition of SCBA should be small too, at least not larger than the variation of CFA produced from coals. Fig. 11 summarizes the chemical compositions of seven SCBA samples and seven class F CFA samples – each includes six randomly selected from the open literature and the one tested in this study. The coefficients of variation (COVs) of major compositions of SCBA, in comparison with CFA, are Na_2O (0.57 vs 0.89), MgO (0.38 vs 0.45), Al_2O_3 (0.44 vs 0.11), SiO_2 (0.11 vs 0.10), CaO (0.33 vs 0.67), Fe_2O_3 (0.37 vs 0.40), and K_2O (0.38 vs 0.44), respectively. It can be seen that the variations of most components of SCBA are smaller than that of CFA, meaning that SCBA can be a more stable material than CFA in the aspect of quality control. The comparison also shows that the CFA and SCBA tested in this study can represent these two types of ashes, and, therefore, the discussions and conclusions drawn from this research are generally meaningful instead of valid only for these two specific ash samples.

The present study has shown the prospective of SCBA to be used as an SCM in portland cement-based materials. First of all, it does not contain spherical particles that provide the ball-bearing effect, so it may not be able to improve the workability of cement-based materials as effectively as CFA. The unburned carbon content of SCBA can be high, and the carbon exists in two forms – nano/submicron carbon particles and micro-scale solid-solution grains which are porous and fragile. These particles may negatively interfere performance of cement-based materials including workability and mechanical performance. Furthermore, SCBA can have a very high glass content comparable to that of class F CFA. However, the glass content of SCBA is dominated by amorphous silica, which is different from CFA that is dominated by amorphous silica and alumina. Therefore, using SCBA as an SCM may result in formation of more secondary C–S–H than using CFA that generates both secondary C–S–H and aluminate hydrates. In addition, because of the vegetable origin of SCBA, it contains much more potassium than CFA, in the forms of solid solution, dissolvable salts and oxides. The high potassium content implies a high risk of alkali-aggregate reaction and the resultant expansion and damage. To sum up, the fine grain size and high glass content of SCBA make it a promising SCM to compensate local demand in sugarcane-producing regions; but it has two drawbacks, that is, potentially high contents of carbon and potassium. Considering the states of carbon and potassium in SCBA, this waste ash can be upgraded by largely removing the adverse matters (Agredo et al., 2014; Souza et al., 2011); and for this purpose, washing, a simple but effective method that has been adopted in upgrading municipal solid waste incineration ashes (Lam et al., 2010), can be employed. In the future, the SCBA may also be classified based on their physicochemical characteristics, similar to the classification of CFA, for its high-efficiency use in cement and concrete industry.

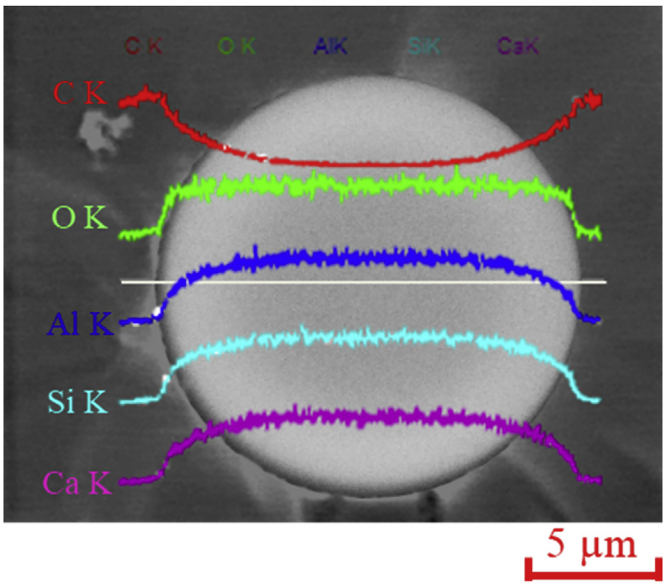

Fig. 10. Distribution of elements in a CFA grain obtained EDS line scanning.

This paper focuses on the prospect of SCBA to be used as an SCM, in terms of composition. In our on-going research, we have been analyzing the pozzolanic reactivity of SCBA and its effects on fresh-/hardened-state properties of cement-based materials. If the reactivity is unsatisfactory, approaches such as grinding and recalcination can be employed to improve the reactivity (Cordeiro et al., 2009, 2018; Souza et al., 2014). These studies will also be benchmarked to class F CFA. The same strategy (as in this paper) of broadly comparing with published data will be employed to discuss the results in a future publication.

Given the chemical composition and physical properties of the SCBA, it may find other value-added applications, such as partially replacement of feedstock for cement production (Amin, 2010; Amin and Ali, 2009), production of activated carbon for pollution control

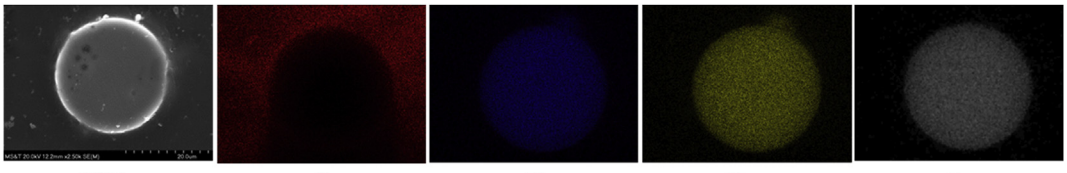

Fig. 9. SEM image of a CFA grain and element mappings based on EDS.

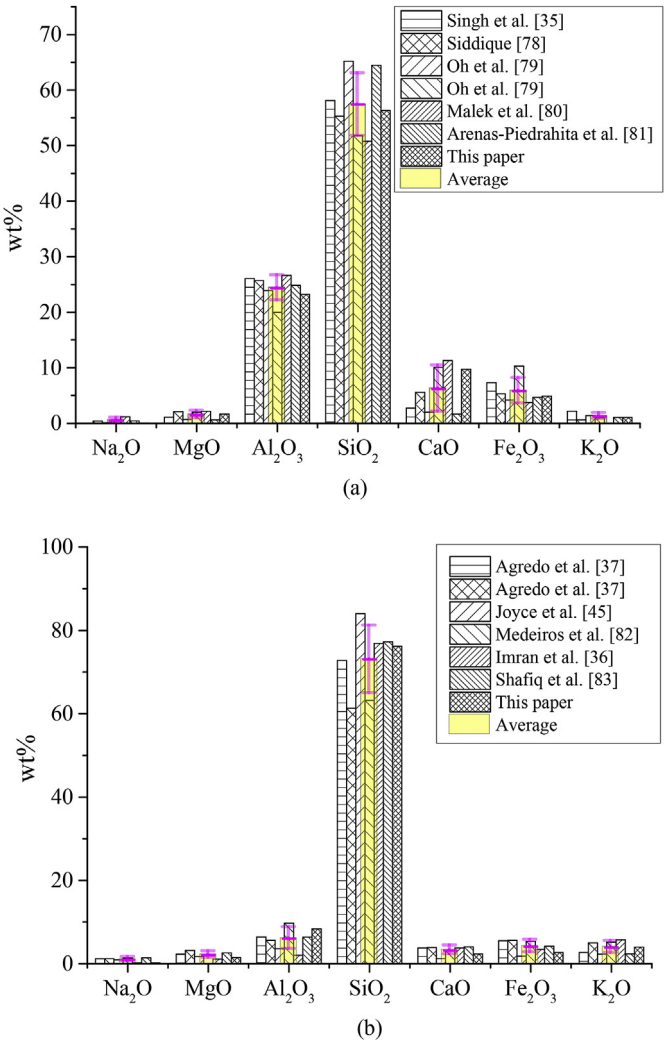

Fig. 11. Compositional variations of SCBA and CFA (Singh and Subramaniam, 2016; Imran and Khan, 2018; Agredo et al., 2014; Joyce et al., 2006; Siddique, 2003; Oh et al., 2014; Malek et al., 2005; Arenas-Piedrahita et al., 2016; de Medeiros et al., 2015; Shafiq et al., 2014): (a) CFA (class F); and (b) SCBA.

(Subramanian et al., 2013; Mendes et al., 2015; Batra et al., 2008), synthesis of silica nanoparticles (Rovani et al., 2018), and proportion of seedling growth media (Webber et al., 2016). These applications are not discussed in detail in this paper.

4. Conclusions

Through a thorough comparison of SCBA and CFA in the light of literature survey and characterization, the prospective of SCBA as a potential SCM to compensate local demand in concrete industry is discussed. The following conclusions can be drawn from this study:

(1) SCBA has fine particle size, high glass content, and relatively stable chemical composition, which means that SCBA is potentially an effective SCM to partially replace portland cement for making concrete.
(2) The glass content of SCBA is dominated by amorphous silica instead of both silica and alumina like in CFA. That is to say, SCBA, when being used as an SCM, tends to result in more secondary C—S—H in the hydration products assembly, instead of both secondary C—S—H and calcium aluminate hydrates in the case of CFA.
(3) Unlike CFA, SCBA contains no spherically shaped silicoaluminate glass grains that can provide ball-bearing effect. In addition, there are a large amount of porous grains in SCBA. Therefore, SCBA may not improve the fresh-state performance of cement-based materials when being used as an SCM; it is more likely to interfere the workability.
(4) As compared to CFA, SCBA contains more unburned carbon and potassium due to its nature of a vegetable ash formed under a lower combustion temperature. Unlike in CFA where carbon is only rich on the surface, carbon in SCBA also broadly exists in some porous grains in the form of graphite. Potassium can exist in the forms of soluble (sulfate and phosphate) salts, oxide, and solid solutions (e.g., with silicoaluminate glass and unburned carbon).
(5) The high carbon and potassium contents of SCBA are potentially detrimental to the fresh-state performance (e.g., workability) and hardened-state properties (e.g., strength and dimension stability compromised due to alkali-aggregate reaction). However, due to the format of existence of the carbon and potassium (i.e., light graphite and dissolvable salts/oxide), these detrimental effects can be mitigated through economically feasible upgrading methods (e.g., washing).

CRediT authorship contribution statement

Ping Zhang: Investigation, Formal analysis, Writing - original draft. **Wenyu Liao:** Investigation, Data curation, Writing - original draft. **Aditya Kumar:** Methodology, Writing - review & editing, Funding acquisition. **Qian Zhang:** Resources, Writing - review & editing. **Hongyan Ma:** Conceptualization, Methodology, Supervision, Writing - review & editing, Funding acquisition.

Declaration of competing interest

The authors declare that they have no known competing financial interests or personal relationships that could have appeared to influence the work reported in this paper.

Acknowledgements

The financial support from National Science Foundation under Grant Nos. CMMI 1661607 and 1761697 is gratefully acknowledged. Any opinions, findings, and conclusions or recommendations expressed in this material are those of the author(s) and do not necessarily reflect the views of the National Science Foundation.

References

Agredo, J.T., de Gutiérrez, R.M., Giraldo, C.E.E., Salcedo, L.O.G., 2014. Characterization of sugar cane bagasse ash as supplementary material for Portland cement. Ing. Invest. 34 (1), 5–10.
Amin, N., 2010. Raw mix designing and clinkerization of High Strength Portland cement with Bagasse Ash and its impact on clinker moduli and fuel consumption. J. Chem. Soc. Pakistan 31 (6), 370.
Amin, N., Ali, K., 2009. Recycling of Bagasse ash in cement manufacturing and its impact on clinker potential and environmental pollution. J. Chem. Soc. Pakistan 31 (3), 357–361.
Arenas-Piedrahita, J., Montes-García, P., Mendoza-Rangel, J., Calvo, H., Valdez-Tamez, P., Martínez-Reyes, J., 2016. Mechanical and durability properties of mortars prepared with untreated sugarcane bagasse ash and untreated fly ash. Construct. Build. Mater. 105, 69–81.
ASTM C1778-19b, 2019. Standard Guide for Reducing the Risk of Deleterious Alkali–Aggregate Reaction in Concrete. ASTM International, West Conshohocken, PA.
ASTM C618-19, 2019. Standard specification for Coal Fly Ash and Raw or Calcined

Natural Pozzolan for Use in Concrete. ASTM International, West Conshohocken, PA.
ASTM D7348-13, 2013. Standard Test Methods for Loss on Ignition (LOI) of Solid Combustion Residues. ASTM International, West Conshohocken, PA.
Bahurudeen, A., Kanraj, D., Dev, V., Santhanam, M., 2015. Performance evaluation of sugarcane bagasse ash blended cement in concrete. Cement Concr. Compos. 59, 77–88.
Batra, V., Urbonaite, S., Svensson, G., 2008. Characterization of unburned carbon in bagasse fly ash. Fuel 87 (13–1), 2972–2976.
Butler, W., Mearing, M., 1985. Fly ash beneficiation and utilization in theory and in practice. Mater. Res. Soc. Symp. Proc. 65, 11–17.
Castaldelli, V., Akasaki, J., Melges, J., Tashima, M., Soriano, L., Borrachero, M., Monzó, J., Payá, J., 2013. Use of slag/sugar cane bagasse ash (SCBA) blends in the production of alkali-activated materials. Materials 6 (8), 3108–3127.
Chancey, R., Stutzman, P., Juenger, M., Fowler, D., 2010. Comprehensive phase characterization of crystalline and amorphous phases of a Class F fly ash. Cement Concr. Res. 40 (1), 146–156.
Cordeiro, G., Kurtis, K., 2017. Effect of mechanical processing on sugar cane bagasse ash pozzolanicity. Cement Concr. Res. 97, 41–49.
Cordeiro, G., Toledo Filho, R., Tavares, L., Fairbairn, E., 2009. Ultrafine grinding of sugar cane bagasse ash for application as pozzolanic admixture in concrete. Cement Concr. Res. 39 (2), 110–115.
Cordeiro, G., Barroso, T., Toledo Filho, R., 2018. Enhancement the properties of sugar cane bagasse ash with high carbon content by a controlled re-calcination process. KSCE Journal of Civil Engineering 22 (4), 1250–1257.
Cordeiro, G., Andreao, P., Tavares, L., 2019. Pozzolanic properties of ultrafine sugar cane bagasse ash produced by controlled burning. Heliyon 5 (10), e02566.
de Medeiros, I., Gomes, K., da Silva, J., 2015. 16th NOCMAT 2015. In: Development of Alkali-Activated Materials Based in Sugarcane Bagasse Ash. Winnipeg, Canada.
Deng, S., Shu, Y., Li, S., Tian, G., Huang, J., Zhang, F., 2016. Chemical forms of the fluorine, chlorine, oxygen and carbon in coal fly ash and their correlations with mercury retention. J. Hazard Mater. 301, 400–406.
Dhengare, S., Raut, S., Bandwal, N., Khangan, A., 2015. Investigation into utilization of sugarcane bagasse ssh as supplementary cementitious material in concrete. International Journal of Emerging Engineering Research and Technology 3 (4), 109–116.
Dhondy, T., Remennikov, A., Shiekh, M., 2019. Benefits of using sea sand and seawater in concrete: a comprehensive review. Aust. J. Struct. Eng. 20 (4), 280–289.
Drozhzhin, V., Shpirt, M., Danilin, L., Kuvaev, M., Pikulin, I., Potemkin, G., Redyushev, S., 2018. Formation processes and main properties of hollow aluminosilicate microspheres in fly ash from thermal power stations. Solid Fuel Chem. 42 (2), 107–119.
Duquiatan, A., Kuykendall, T., Sweeney, D., Thomas, L., 2020. US power generators set for another big year in coal plant closures in. S&P Global Market Intelligence, 13 January 2020 [Online]. Available: https://www.spglobal.com/marketintelligence/en/news-insights/latest-news-headlines/56496107. Accessed 7 May 2020.
Estrade-Szwarckopf, H., 2004. XPS photoemission in carbonaceous materials: a "defect" peak beside the graphitic asymmetric peak. Carbon 42 (8–9), 1713–1721.
Fairley, N., 2009. CasaXPS Manual 2.3. 15: Introduction to XPS and AES. In: XPS Spectra. Casa Software Ltd.
Fleischman, L., Cleetus, R., Deyette, J., Clemmer, S., Frenkel, S., 2013. Ripe for retirement: an economic analysis of the U.S. coal fleet. Electr. J. 26 (10), 51–63.
A. A. Frey, N. R. Wozniak, T. B. Nagi, M. P. Keller, J. M. Lunderberg, G. F. Peaslee, P. A. DeYoung and J. R. Hampton, "Analysis of electrodeposited nickel-iron alloy film composition using particle-induced X-ray emission," International Journal of Electrochemistry, vol. 2011, 2011.
Fu, B., Hower, J., Dai, S., Mardon, S., Liu, G., 2018. Determination of chemical speciation of arsenic and selenium in high-as coal combustion ash by X-ray photoelectron spectroscopy: examples from a Kentucky stoker ash. ACS Omega 3 (12), 17637–17645.
Ganesan, K., Rajagopal, K., Thangavel, K., 2007. Evaluation of bagasse ash as supplementary cementitious material. Cement Concr. Compos. 29 (6), 515–524.
Ha, J., Chae, S., Chou, K., Tyliszczak, T., Monteiro, P., 2016. Characterization of class F fly ash using STXM. J. Nanomater. 63.
Hemalatha, T., Mapa, M., George, N., Sasmal, S., 2016. Physico-chemical and mechanical characterization of high volume fly ash incorporated and engineered cement system towards developing greener cement. J. Clean. Prod. 125, 268–281.
Hu, C., Ma, H., 2016. Statistical analysis of backscattered electron image of hydrated cement paste. Adv. Cement Res. 28 (7), 469–474.
Ibáñez, J., Font, O., Moreno, N., Elvira, J., Alvarez, S., Querol, X., 2013. Quantitative Rietveld analysis of the crystalline and amorphous phases in coal fly ashes. Fuel 105, 314–317.
Imran, M., Khan, A., 2018. Characterization of agricultural waste sugarcane bagasse ash at 1100° C with various hours. Mater. Today: Proceedings 5 (2), 3346–3352.
Joyce, J., Dixon, T., Diniz da Costa, J., 2006. Characterization of sugar cane waste biomass derived chars from pressurized gasification. Process Saf. Environ. Protect. 84 (6), 429–439.
Juenger, M.C., Winnefeld, F., Provis, J.L., Ideker, J.H., 2011. Advances in alternative cementitious binders. Cement Concr. Res. 41, 1232–1243.
Külaots, I., Hurt, R., Suuberg, E., 2004. Size distribution of unburned carbon in coal fly ash and its implications. Fuel 83 (2), 223–230.
Kutchko, B., Kim, A., 2006. Fly ash characterization by SEM–EDS. Fuel 85 (17–18), 2537–2544.
Lam, C.H.K., Ip, A.W.M., Barford, J.P., McKay, G., 2010. Use of incineration MSW ash: a review. Sustainability 2, 1943–1968.
LC3, 2014. Limestone Calcined Clay Cement. LC3 Project Office [Online]. Available: https://www.lc3.ch/.
Le Saoût, G., Kocaba, V., Scrivener, K., 2011. Application of the Rietveld method to the analysis of anhydrous cement. Cement Concr. Res. 41 (2), 133–148.
Liao, W., Ma, H., Sun, H., Huang, Y., Wang, Y., 2017. Potential large-volume beneficial use of low-grade fly ash in magnesia-phosphate cement based materials. Fuel 209, 490–497.
Liao, W., Kumar, A., Khayat, K., Ma, H., 2019a. Multifunctional lightweight aggregate containing phase change material and water for damage mitigation of concrete. ES Materials and Manufacturing 6, 49–61.
Liao, W., Sun, X., Kumar, A., Sun, H., Ma, H., 2019b. Hydration of binary portland cement blends containing silica fume: a decoupling method to estimate degrees of hydration and pozzolanic reaction. Frontiers in Materials 6 (13), 78.
Liu, F., Li, W., Guo, H., Li, B., Bai, Z., Hu, R., 2011. XPS study on the change of carbon-containing groups and sulfur transformation on coal surface. J. Fuel Chem. Technol. 39 (2), 81–84.
Ma, H., 2013. Multi-Scale Modeling of the Microstructure and Transport Properties of Contemporary Concrete. PhD Thesis. the Hong Kong University of Science and Technology, Hong Kong.
Malek, R., Khalil, Z., Imbaby, S., Roy, D., 2005. The contribution of class-F fly ash to the strength of cementitious mixtures. Cement Concr. Res. 35 (6), 1152–1154.
Massazza, F., 1998. Lea's Chemistry of Cement and Concrete, fourth ed. In: Pozzolana and Pozzolanic Cements. Butterworth-Heinemann, Oxford, UK, pp. 471–631.
Mendes, F., Marques, A., Mendonça, D., Oliveira, M., Moutta, R., Ferreira-Leitão, V., 2015. High surface area activated carbon from sugar cane straw. Waste and Biomass Valorization 6 (3), 433–440.
Monteiro, P., Miller, S., Horvath, A., 2017. Towards sustainable concrete. Nat. Mater. 16 (7), 698–699.
Moraes, J., Akasaki, J., Melges, J., Monzó, J., Borrachero, M., Soriano, L., Payá, J., Tashima, M., 2015. Assessment of sugar cane straw ash (SCSA) as pozzolanic material in blended Portland cement: microstructural characterization of pastes and mechanical strength of mortars. Construct. Build. Mater. 94, 670–677.
Murakami, Y., Kishimoto, T., Suematsu, H., 1990. Structures of high-stage donor-acceptor hetero-structure graphite intercalation compounds. J. Phys. Soc. Jpn. 59 (2), 571–578.
Naumkin, A., Kraut-Vass, A., Gaarenstroom, S., Powell, C., 2012. NIST X-ray photoelectron spectroscopy database. NIST Standard Reference Database 20. Version 4.1.
Neville, A., 2011. Properties of Concrete, fifth ed. Prentice Hall, Upper Saddle River, New Jersey.
Oh, J., Jun, Y., Jeong, Y., 2014. Characterization of geopolymers from compositionally and physically different Class F fly ashes. Cement Concr. Compos. 50, 16–26.
Ohki, A., Nakajima, T., Sakaguchi, Y., Iwashita, A., Takanashi, H., 2005. Analysis of arsenic and some other elements in coal fly ash by X-ray photoelectron spectroscopy. J. Hazard Mater. 119 (1–3), 213–217.
Pande, G., Selvakumar, S., Batra, V., Gardoll, O., Lamonier, J., 2012. Unburned carbon from bagasse fly ash as a support for a VOC oxidation catalyst. Catal. Today 190 (1), 47–53.
Pereira, P., Voorwald, H., Cioffi, M., Da Silva, M., Rego, A., Ferraria, A., De Pinho, M., 2014. Sugarcane bagasse cellulose fibres and their hydrous niobium phosphate composites: synthesis and characterization by XPS, XRD and characterization by XPS, XRD and SEM. Cellulose 21 (1), 641–652.
Pereira, A., Akasaki, J., Melges, J., Tashima, M., Soriano, L., Borrachero, M., Monzó, J., Payá, J., 2015. Mechanical and durability properties of alkali-activated mortar based on sugarcane bagasse ash and blast furnace slag. Ceram. Int. 41 (10), 13012–13024.
Rajamma, R., Ball, R., Tarelho, L., Allen, G., Labrincha, J., Ferreira, V., 2009. Characterisation and use of biomass fly ash in cement-based materials. J. Hazard Mater. 172 (2–3), 1049–1060.
Rerkpiboon, A., Tangchirapat, W., Jaturapitakkul, C., 2015. Strength, chloride resistance, and expansion of concretes containing ground bagasse ash. Construct. Build. Mater. 101, 983–989.
Reyes-Herrera, J., Miranda, J., De Lucio, O., 2015. Simultaneous PIXE and XRF elemental analysis of atmospheric aerosols. Microchem. J. 120, 40–44.
Rivera, F., Martínez, P., Castro, J., López, M., 2015. Massive volume fly-ash concrete: a more sustainable material with fly ash replacing cement and aggregates. Cement Concr. Compos. 63, 104–112.
Rovani, S., Santos, J., Corio, P., Fungaro, D., 2018. Highly pure silica nanoparticles with high adsorption capacity obtained from sugarcane waste ash. ACS Omega 3 (3), 2618–2627.
Scrivener, K.L., John, V.M., Gartner, E.M., 2018. Eco-efficient cements: potential economically viable solutions for a low-CO2 cement-based materials industry. Cement Concr. Res. 114, 2–26.
Shafiq, N., Elhsameed, A., Nuruddin, M., 2014. Durability of sugar cane bagasse ash (SCBA) concrete towards chloride ion penetration. Appl. Mech. Mater. 567, 369–374.
Shen, D., Zhang, Y., 1981. A study of the effects of fly ash (in Chinese). J. Chin. Ceram. Soc. 9 (1), 57–63.
Shi, C., Day, R., 2000. Pozzolanic reaction in the presence of chemical activators: Part II—reaction products and mechanism. Cement Concr. Res. 30 (4), 607–613.

Siddique, R., 2003. Effect of fine aggregate replacement with Class F fly ash on the abrasion resistance of concrete. Cement Concr. Res. 33 (11), 1877–1881.
Singh, G., Subramaniam, K., 2016. Quantitative XRD study of amorphous phase in alkali activated low calcium siliceous fly ash. Construct. Build. Mater. 124, 139–147.
Souza, A., Teixeira, S., Santos, G., Costa, F., Longo, E., 2011. Reuse of sugarcane bagasse ash (SCBA) to produce ceramic materials. J. Environ. Manag. 92 (10), 2774–2780.
Souza, L., Fairbairn, E., Toledo Filho, R., Cordeiro, G., 2014. Influence of initial CaO/SiO2 ratio on the hydration of rice husk ash-Ca(OH)2 and sugar cane bagasse ash-Ca(OH)2 pastes. Quím. Nova 37 (10), 1600–1605.
Subramanian, S., Pande, G., Weireld, D., Giraudon, J., Lamonier, J., Batra, V., 2013. Sugarcane bagasse fly ash as an attractive agro-industry source for VOC removal on porous carbon. Ind. Crop. Prod. 49, 108–116.
Thomas, M., Jewell, R., Jones, R., 2017. Coal Combustion Products (CCP's): Characteristics, Utilization and Beneficiation. In: Coal Fly Ash as a Pozzolan. Woodhead Publishing, Cambridge, UK, pp. 121–154.
TRB, 2018. NCHRP 10-104 - Recommendations for Revision of AASHTO M 295 Standard Specification to Include Marginal and Unconventional Source Coal Fly Ashes [Online]. Available: https://apps.trb.org/cmsfeed/TRBNetProjectDisplay.asp?ProjectID=4565. Accessed 2 12 2019.
United Staes Department of Agriculture, 2015. Sugar: World Markets and Trade. United Staes Department of Agriculture, Foreign Agricultural Service.
Usman, A., Raji, A., Waziri, N., Hassan, M., 2014. A study on silica and alumina potential of the savannah bagasse ash. IOSR J. Mech. Civ. Eng. 11 (3), 48–52.
Vander Wal, R., Bryg, V., Hays, M., 2011. XPS analysis of combustion aerosols for chemical composition, surface chemistry, and carbon chemical state. Anal. Chem. 83 (6), 1924–1930.
Webber III, C., White Jr., P., Petrie, E., Shrefler, J., Taylor, M., 2016. Sugarcane bagasse ash as a seedling growth media component. J. Agric. Sci. 8 (1), 1–7.
Wyatt, P., 1980. Some chemical, physical, and optical properties of fly ash particles. Appl. Optic. 19 (6), 975–983.
Xu, G., Shi, X., 2018. Characteristics and applications of fly ash as a sustainable construction material: a state-of-the-art review. Resour. Conserv. Recycl. 136, 95–109.
Yan, K., Guo, Y., Ma, Z., Zhao, Z., Cheng, F., 2018. Quantitative analysis of crystalline and amorphous phases in pulverized coal fly ash based on the Rietveld method. J. Non-Cryst. Solids 483, 37–42.
Zevenbergen, C., Bradley, J., Van Reeuwijk, L., Shyam, A., Hjelmar, O., Comans, R., 1999. Clay formation and metal fixation during weathering of coal fly ash. Environ. Sci. Technol. 33 (19), 3405–3409.
Żyrkowski, M., Neto, R., Santos, L., Witkowski, K., 2016. Characterization of fly-ash cenospheres from coal-fired power plant unit. Fuel 174, 49–53.